ELSEVIER

Journal of Neuroscience Methods 168 (2008) 54–63

JOURNAL OF NEUROSCIENCE METHODS

www.elsevier.com/locate/jneumeth

A simulation study for a surface EMG sensor that detects distinguishable motor unit action potentials

Jin Lee [a,*], Alexander Adam [b], Carlo J. De Luca [b,c]

[a] *Department of Control & Instrumentation Engineering, Kangwon National University, KyoDong Samcheok KangwonDo 245-711, Republic of Korea*

[b] *NeuroMuscular Research Center, Boston University, Boston, MA 02215, USA*

[c] *Department of Biomedical Engineering, Boston University, Boston, MA 02215, USA*

Received 28 June 2007; received in revised form 21 August 2007; accepted 11 September 2007

Abstract

An advanced volume conductor model was used to simulate the surface-detected motor unit action potentials (MUAPs) due to current sources located at different depths within the muscle tissue of the biceps brachii. Seven different spatial filters were investigated by linear summation of the monopolarly detected surface MUAPs on a square array of nine electrodes. The criterion of the relative energy-of-difference (EOD) between the MUAPs was used to rank spatial filters for their ability to distinguish two motor units located at different depths. Using the same criterion pair wise combinations of spatial filters were ranked for their ability to generate different MUAP shape representations of the same motor unit. In both analyses, the bi-transversal double-differential (BiTDD) configurations and pair wise combinations involving a BiTDD configuration consistently ranked highest. Varying electrode spacing did not change the results in a relevant way. Based on the EOD calculations, a four-channel detection system using all available electrodes of the array is proposed. The implications of using only six electrodes, effectively reducing contact area of the sensor in half, are discussed.

Keywords: Surface electromyography; Electrode array; Motor unit; Spatial filter

1. Introduction

During the past three decades there have been several attempts at developing techniques and technologies for decomposing the electromyographic (EMG) signal into the constituent action potentials (Broman, 1988; De Luca and Adam, 1999; De Luca and Forrest, 1972; Fang et al., 1999; Hochstein et al., 2002; LeFever and De Luca, 1982; LeFever et al., 1982; Mambrito and De Luca, 1984; McGill et al., 1985; Nawab et al., 2004a,b; Stashuk and de Bruin, 1988; Zennaro et al., 2001). These have attained varying degrees of success. The difficulty of obtaining successful and useful decompositions of EMG signals that contain more than three motor units is such that only signals detected by indwelling sensors, which are inherently the most selective, have been attempted. These indwelling sensors have various forms such as the commonly used monopolar needle sensor (McGill et al., 1985), the quadrifilar needle sensor (De Luca and Adam, 1999; De Luca and Forrest, 1972; LeFever and De Luca, 1982) and more recently the quadrifilar wire sensor, that are inserted via a needle (De Luca and Adam, 1999). The latter two sensors are used with our own decomposition technique, called precision decomposition (De Luca and Adam, 1999; LeFever et al., 1982; Mambrito and De Luca, 1984).

The EMG signal decomposition studies performed with indwelling sensors have proved to be fruitful for physiological and clinical investigations. Physiological investigations (Adam and De Luca, 2005; LeFever and De Luca, 1982; LeFever et al., 1982; Mambrito and De Luca, 1984) have provided considerable knowledge about the common behavior of concurrently active motor units that has given new insight to the mechanisms used by the CNS to regulate the production of force in the muscle. Clinical investigations have provided new knowledge of motor control in the aging CNS (Erim et al., 1999) and in acute cerebellar stroke (Sauvage et al., 2006). However, indwelling sensors have obvious limitations that considerably restrict their usability. For example, needle sensors cause discomfort, especially for children and elderly. Consequently they are not typically used for recording sessions of more than a few minutes duration and

* Corresponding author. Tel.: +82 33 570 6386; fax: +82 33 570 6389.
E-mail address: jlee@kangwon.ac.kr (J. Lee).

0165-0270/$ – see front matter © 2007 Elsevier B.V. All rights reserved.
doi:10.1016/j.jneumeth.2007.09.007

often require re-insertions to obtain a high quality signal that is a candidate for decomposition. If not used properly, they have the potential of transmitting various diseases. They invariably migrate during a contraction, even an isometric constant force contraction, causing change in the shape and amplitude of the action potentials. This alteration can cause havoc in the algorithms that are used for decomposing the EMG signals, resulting in failure. Also, they may cause damage to the muscle fibers in the proximity of the sensor and small blood pools in the vicinity of the detection surfaces can cause dramatic deterioration of the quality of the signal.

For those muscles that are not in contact with the skin, the needle sensor remains the only viable option. However, for the rest it would be preferable to be able to decompose the EMG signal detected from a surface sensor. The purpose of this study was to design a surface EMG sensor that could be used with our precision decomposition technique. Recent improvements (Hochstein et al., 2002; Nawab et al., 2004a) to the algorithms have resulted in higher accuracy (>95%) and a short time to decomposition (<8 times acquisition time), making it suitable for clinical purposes. This recent version would benefit from a surface sensor.

Herein we describe an approach for designing a surface sensor based on a two-dimensional electrode array that would suit the purpose. Although two-dimensional electrode arrays were proposed more than 15 years ago (Reucher et al., 1987a,b) and a number of subsequent studies investigated their performance (Dimitrov et al., 2003; Disselhorst-Klug et al., 1997; Farina and Cescon, 2001; Farina and Merletti, 2001; Farina and Rainoldi, 1999; Farina et al., 2002, 2003, 2004; Helal and Bouissou, 1992; Östlund et al., 2004; Schneider et al., 1991; among others), none have explored their suitability for discriminating amongst the shapes of the detected action potentials.

2. Methods

In developing the approach for designing the electrode array sensor, we focused on maximizing the difference in shape and amplitude of the motor unit action potentials (MUAPs) in the EMG signal that would be detected. The efficacy of the sensor was assessed by the following two criteria. First, which spatial filter maximizes the shape difference between two MUAPs? Second, which multi-channel configuration of spatial filters maximizes the shape difference between two different channels? We used the energy-of-difference (EOD), a variation of the standard measure of the difference in energy (Oppenheim and Schafer, 1975), to quantify the shape difference between two mathematically generated MUAPs.

2.1. The model

We used an advanced analytical volume conductor model developed by Blok et al. (2002) to evaluate several array configurations. The model can generate single MUAPs resulting from the linear summation of bioelectric sources in a finite, cylindrical, and anisotropic volume conductor that consists of three layers, representing muscle, subcutaneous fat, and skin tissue. While the model can accommodate any current-density source, we chose to adopt the analytical expression of the intracellular action potential (IAP) proposed by Rosenfalck (Andreassen and Rosenfalck, 1978), although other analytical source expressions exist in the literature (Griep et al., 1982; McGill et al., 2001; Merletti et al., 1999a,b). Previous studies (Blok et al., 2002; Farina et al., 2002) have shown that the Rosenfalck source closely matched real signals and that differences among MUAPs generated by other commonly used source functions were small. The IAP is given as voltage $V(z)$, where z is the spatial dimension along the fiber:

$$V(z) = 96z^3\exp(-z) - 90\,[\mathrm{mV}] \quad (1)$$

The model was used to calculate the monopolar MUAP at a point along the outer surface (skin) of the volume conductor. An overview of the model geometry and important parameters for the simulation are provided in Fig. 1 and Table 1, respectively. The choice of model parameter values reflects the anatomy of the biceps brachii muscle (Basmajian and De Luca, 1985; Masuda et al., 1985) and commonly used muscle, fat, and skin tissue prop-

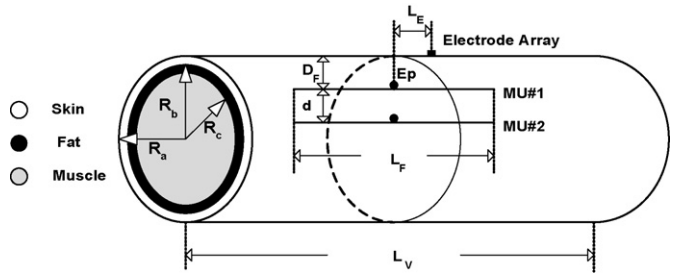

Fig. 1. The model configuration for the simulation of surface-detected MUAPs. A three-layer cylindrical volume conductor was used to represent muscle, fat, and skin tissue. The center of the surface electrode array was positioned at longitudinal distance L_E from the midline of the cylinder and detected the electrical activity of two motor units located at depths D_F and $D_F + d$ below the skin. See Table 1 for a description of additional model parameters.

Table 1
Selected model parameters to generate the MUAP signals

Description of the parameter (symbol)	Default value
Radius of muscle compartment (R_c) (mm)	38
Radius of fat + muscle compartment (R_b) (mm)	39
Volume conductor radius (R_a) (mm)	40
Volume conductor length (L_v) (mm)	200
Conductivity of muscle compartment, axial ($\Omega\,m^{-1}$)	0.5
Conductivity of muscle compartment, radial ($\Omega\,m^{-1}$)	0.1
Conductivity of fat compartment ($\Omega\,m^{-1}$)	0.05
Conductivity of skin compartment ($\Omega\,m^{-1}$)	1.0
Muscle fibers belonging to one motor unit	200
Muscle fiber conduction velocity (m/s)	3.125
Mean fiber length (L_F) (mm)	100, S.D. = 20
Electrode array distance (L_E) from mean endplate position (mm)	20
Mean end plate position (E_P) (mm)	0, S.D. = 10
Mean tendon position (mm)	±50, S.D. = 10
Sample frequency (Hz)	2000
Muscle fiber depth (D_F) of MU#1 (mm)	3–5; 3–13
Difference in depth (d) between MU#1 and MU#2 (mm)	1–10

erties (Blok et al., 2002; Disselhorst-Klug et al., 1998; Farina and Rainoldi, 1999; Roeleveld et al., 1997).

As shown in Fig. 1, the source fibers (200/motor unit) lie parallel to the cylinder axis (z direction) with the motor endplates (the innervation region of the muscle fibers) in the middle of the cylinder. All source fibers belonging to the same motor unit were located at the same depth below the skin, but differed in the position of the endplate and the tendon insertion, and thus fiber length. The tendon and endplate positions of the fibers were drawn at random from a normal distribution (tendon: mean = ±50 mm, S.D. = 10; endplate: mean = 0 mm, S.D. = 10). The central electrode of the array was located above the fiber axis at an axial distance of $L_E = 20$ mm from the mean endplate position. The location of motor units below the skin was defined as the depth of motor unit #1, D_F, and the incremental depth of motor unit #2, $D_F + d$. With this fixed simulation setup we generated all the MUAPs while only varying the depth parameters. The range of motor unit depths (3–15 mm) was selected by considering practically useful values for SEMG in the biceps brachii.

2.2. The detection system

A comparison of different types of spatial filters configurations was obtained by calculating monopolar MUAP signals detected on a square grid of nine point electrodes. These monopolar MUAP signals were then selected and summed, using appropriate weights for each electrode, to derive the spatial filter configurations. The following types of spatial filters were investigated: the longitudinal single differential (LSD), the transversal single differential (TSD), the longitudinal double differential (LDD), the transversal double differential (TDD), the normal double differential (NDD) (Reucher et al., 1987b; Farina et al., 2003), the bi-transversal double differential (BiTDD) (Dimitrov et al., 2003), and the inverse binomial of order two (IB2) (Disselhorst-Klug et al., 1997). Fig. 2 shows the electrode arrangements and the filter coefficients for each of these seven types of spatial filters. The figure also indicates every possible arrangement for each of the spatial filter configurations that can be derived from the array of nine electrodes. In total, 22 configurations can be formed. Because of the symmetry of the simulation setup around the center row of electrodes, which are aligned with the motor unit axes, we only report on 16 different configurations (Table 3).

2.3. Criterion for assessing the difference between two MUAPs

The aim of this study was to investigate which spatial filter configuration maximizes the difference in MUAP shape between two different motor units. From the preliminary data analysis and the review of previous work by Dimitrov et al. (2003), Farina et al. (2002) and Dimitrova et al. (1999) we found that the factors that contributed most to the difference in MUAP shape between motor units were waveform amplitude and duration. Thus, we have selected the relative energy-of-difference (EOD) defined by Eq. (2) as the criterion for measuring MUAP shape differences.

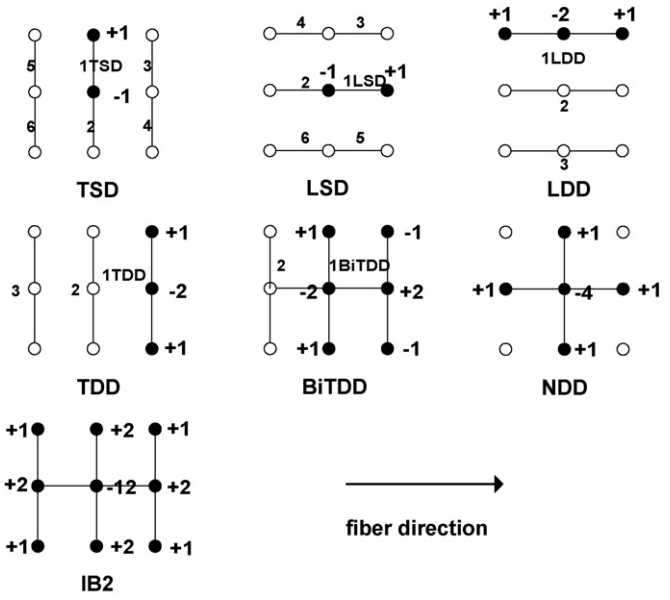

Fig. 2. A schematic representation of the spatial filter configurations on a nine-electrode grid aligned with respect to the muscle fiber direction. Bold connection lines indicate the electrodes used for a single realization. Signed, bold numbers indicate the weighting factors of the electrodes. Unsigned numbers indicate the numbering of configurations if alternative arrangements were realized. All the electrodes are dimensionless points and are positioned on a grid with the same inter-electrode distance. The abbreviations for spatial filter configurations are: LSD, longitudinal single differential; TSD, transversal single differential; LDD, longitudinal double differential; TDD, transversal double differential; BiTDD, bi-transversal double differential; NDD, normal double differential; IB2, second order inverse binominal.

$$\mathrm{EOD} = \frac{\int_0^T |S1(t) - S2(t)|^2 \, \mathrm{d}t}{\int_0^T \{|S1(t)|^2 + |S2(t)|^2\} \, \mathrm{d}t} \tag{2}$$

where $S1(t)$ and $S2(t)$ are MUAP time series in the interval 0 to $T = 25$ ms generated from MU#1 and MU#2, respectively. The EOD value is the energy of the point-by-point difference between $S1(t)$ and $S2(t)$ relative to the sum of their individual energies. The EOD is sensitive to differences in the amplitude as a function of time. By simply computing the difference in the energy of each signal one would lose the timing information. Since differences in timing and shape are critical to detect shape difference between two signals, we opted for the standard measure to compute such differences. A higher value of the EOD represents a greater difference between the MUAPs of two motor units.

3. Results

3.1. Example MUAP waveforms

Fig. 3 shows examples of MUAP signals detected by seven different spatial filter configurations that were derived from nine electrodes spaced on a 2.3 mm grid. Each graph consists of two MUAP signals originating from two different motor units located at 3 mm (MU#1) and 5 mm (MU#2) below the skin. Each signal was normalized with respect to the peak amplitude of the

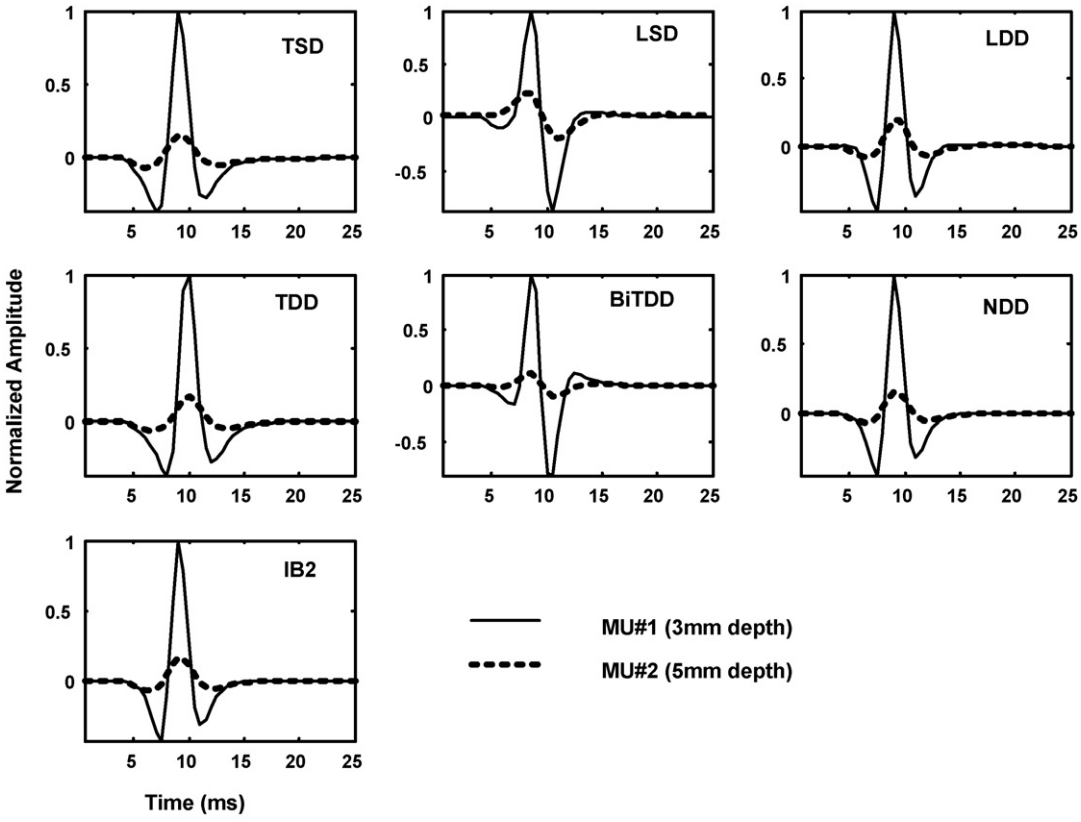

Fig. 3. Examples of simulated MUAP signals detected by the seven different spatial filters. The signals from single differential (TSD, LSD), double differential (LDD, TDD) and more complex (BiTDD, NDD, IB2) spatial filter configurations are shown. Each graph contains two MUAP signals originating from two different motor units, located depths of 3 mm and 5 mm below the skin. The MUAPs of MU#1 (solid line) and MU#2 (dotted line) were normalized by the peak amplitude of MU#1. The position of the electrode array on the skin surface was fixed at an axial distance $L_E = 20$ mm from the endplate region. Other parameters of the simulation are indicated in Table 1 and Fig. 1.

MUAP of MU#1 for easy comparison. (See Fig. 1 for additional details of this simulation.)

The graphs in Fig. 3 illustrate the difference in MUAP shape, amplitude and duration for two motor units located at different depths. We chose to plot the results for a depth difference of $d = 2$ mm because at that depth difference the EOD values exhibited the largest variation among the several electrode configurations. The attenuation of the amplitude of the deeper motor unit (MU#2) depended on the spatial filter, as indicated by several previous studies. (Dimitrov et al., 2003; Farina et al., 2002, 2003). In order to evaluate the difference in MUAP shape quantitatively, we calculated traditional EMG variables: signal amplitude (positive peak), duration (time from generation to extinction), and energy (Table 2). These variables are expressed as the percentage difference between MU#1 and MU#2 values. In addition, the energy of difference (EOD) in MUAP waveforms was obtained by Eq. (2).

The increased fiber depth of MU#2 in comparison to MU#1 resulted in an equal or increased duration of its MUAP, but decreased peak amplitude and energy, for every spatial filter configuration tested (Table 2). The shortest duration MUAP of MU#1, the superficial motor unit, was 12.5 ms, estimated from the NDD and the BiTDD detection. The shortest MUAP of MU#2, the deeper motor unit, was 15.5 ms, estimated from

Table 2
Evaluation of EMG variables of Fig. 3

Spatial filter	Duration (ms) %, (MU#1/MU#2)	Peak amplitude (mV) %, (MU#1/MU#2)	Energy %	EOD
TSD	2.8 (18/18.5)	−84.7 (0.52/0.08)	−96.2	0.67
LSD	0 (19/19)	−78.7 (0.14/0.03)	−92.0	0.56
LDD	5.6 (18/19)	−80.5 (0.11/0.02)	−94.4	0.62
TDD	0 (19/19)	−83.7 (0.10/0.02)	−95.8	0.67
BiTDD	40 (12.5/17.5)	−89.5 (0.83/0.09)	−98.3	0.79
NDD	36 (12.5/17)	−84.6 (0.27/04)	−96.3	0.69
IB2	19.2 (13/15.5)	−83.7 (0.12/0.02)	−95.8	0.67

The duration, amplitude and energy are given as a % difference between MU#1 and MU#2 (located at a depth of 3 mm and 5 mm, respectively). Absolute values of the EMG variables are shown in parentheses. The EOD was calculated by Eq. (2).

the IB2 configuration. The percent difference in peak amplitude between the two MUAPs was greater than 80% for six out of seven spatial filter configurations, even through the signals originated from two motor units located only 2 mm apart in depth. Similarly, the energy attenuation between MU#1 and MU#2 was greater than 90% for all signals. The EOD value, which was used as the main criterion in this simulation, presented the same trend of variation as the energy attenuation. Overall, the BiTDD detection presented the largest peak amplitude difference (89.5%), energy attenuation (98.3%), and EOD (0.79) (Table 2).

3.2. Effect of varying the difference in the relative depth of two motor units

Fig. 4A presents the EOD between the MUAP signals of two motor units as a function of spatial filter configuration and motor unit location (depth difference between MU#1 and MU#2). Here, the depth of MU#1, D_F, was fixed at 3 mm while that of MU#2, $D_F + d$, varied in 1 mm increments from 4 mm to 13 mm. The figure shows that increasing the depth difference, d, increased the EOD value for every spatial filter configuration. The EOD value ranged from 0.14 at the smallest depth difference investigated ($d = 1$ mm) to 0.99 at the largest difference ($d = 10$ mm). The variation of the EOD among the spatial filter configurations decreased as the depth difference increased. (Note however, that the variation of EOD at $d = 2$ mm is higher than that at $d = 1$ mm.) This result shows that the EOD between a superficial and a deep motor unit ($d > 2$ mm) is affected less by the spatial filter than that between two superficial motor units ($d \leq 2$ mm). In line with the work of Gydikov et al. (1982), Farina et al. (2002) and Ferdjallah et al. (1999), it is noted that the anatomical characteristics of the motor unit, such as depth below the skin, have more impact on the surface-detected MUAP than the characteristics of the spatial filter. In the case of the TSD and TDD filters, the EOD showed similar values for the different configurations but there was a consistent variation in the EOD among the LSD and LDD configurations; the longitudinal configurations located lateral to the fiber axis (i.e. 3LSD, 4LSD, 1LDD) had lower EOD values than those located centrally. Thus, the longitudinal detection scheme was the one most affected by the detection position. Note that, across all simulation results, the EOD values for the two BiTDD configurations were always at least 10% greater than those of the other configurations. Based on this criterion, the BiTDD spatial filter configurations were the best for maximizing the energy difference between two MUAPs for all motor unit depth difference simulated in this study.

3.3. Effect of varying the electrode spacing

The influence of electrode spacing on EOD values between the MUAPs of two motor units for different spatial filters was investigated for three spacing values: 1.6 mm, 2.3 mm (used as a default spacing in this study), and 3.1 mm. These values were chosen because they allow for a small electrode array that can be used on small muscles of the hand and face as well as all other large muscles, such as the biceps brachii. As Fig. 4A illustrates, the trend in EOD variation for each spatial filter did not change by using different spacing values. The MUAPs of two motor units detected with the two BiTDD configurations always showed the highest shape difference, as measured by the EOD, and those detected with the LSD configurations the lowest in all conditions. Overall, the EOD values decreased with increased

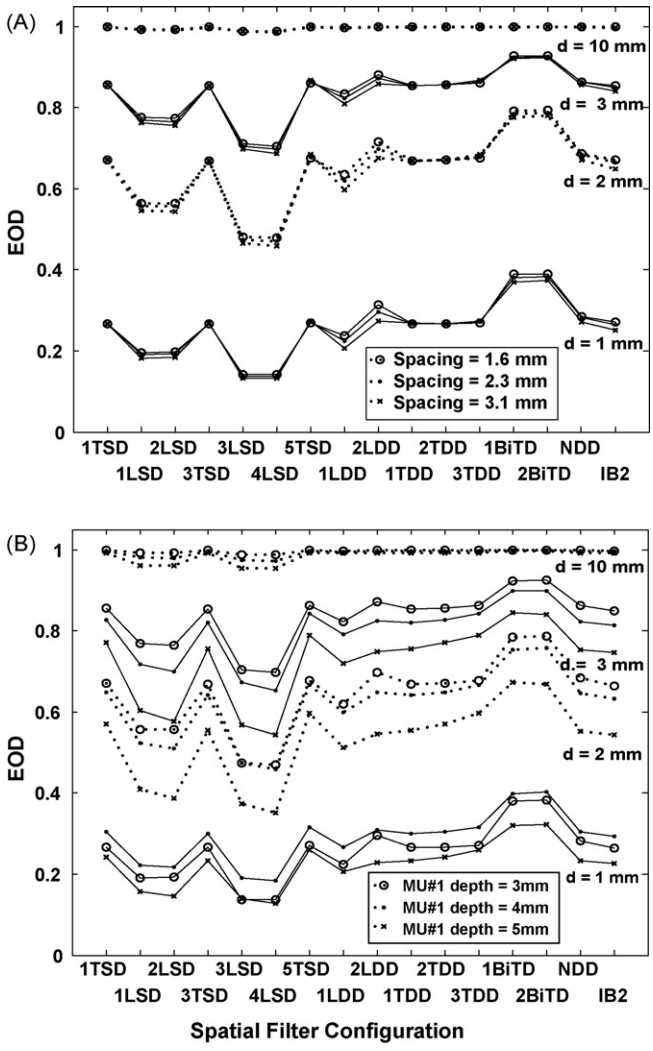

Fig. 4. (A) The estimation of the relative energy-of-difference (EOD) as a function of electrode spacing and difference in fiber depth for each spatial filter configuration. Every EOD value was calculated from the MUAP signals from two different motor units (MU#1 and MU#2). MU#1 was fixed at a depth of 3 mm below the skin and the location of MU#2 varied from 4 mm to 13 mm in 1 mm steps. Dashed lines connect EOD values from the same depth difference (d) as indicated on the right. For clarity, only results for four depth differences (1, 2, 3, and 10 mm) are shown. For example, the graph tagged by "$d = 1$ mm" contains the information for MU#1 and MU#2 located at depths of 3 mm and 4 mm. The labels on the x-axis indicate the different spatial filter configurations (see Fig. 2) and are ordered by increasing complexity of implementation. The EOD values for three different electrode spacing values (1.6 mm, 2.3 mm, 3.1 mm) are plotted with different symbols (circle, dot, cross). (B) The EOD values plotted as a function of spatial filter configuration for different ranges of motor unit depths. The EOD values for the three different sets of depths were calculated as in (A) with the electrode array spacing fixed at 2.3 mm. To investigate the three depth ranges, the depth of MU#1 was fixed at 3 mm (circles), 4 mm (dots), or 5 mm (circles) while the depth of MU#2 varied from 4 mm to 13 mm, 5 mm to 14 mm, or 6 mm to 15 mm, respectively, in 1 mm increments. Note that for clarity, only four depth differences are plotted. BiTD = BiTDD.

spacing but the relative change in EOD between average values at 1.6 mm and at 3.1 mm spacing was less than 3.5% (overall mean decrease = 1.5%) for each spatial filter. In particular, the EOD between the signals from the 1TSD, 3TSD, and 5TSD, as well as the 1TDD and 2TDD configurations were nearly identical for all of three spacing values. The results of this simulation indicate that the EOD changed little in the investigated spacing range.

3.4. Effect of variation in motor unit depth

Fig. 4B shows the behavior of the EOD of pairs of MUAPs whose motor units differ in location but had the same depth difference (d). In all cases the highest EOD was always obtained from the BiTDD detection. For any given depth difference, except at $d = 1$ mm, the EOD was generally higher the closer MU#1 was to the electrode array. Note that the EOD variation was larger for the range of motor unit depths (Fig. 4B) than for the range of contact pin spacing values (Fig. 4A). This is another indication of the observation that the anatomical location of the two motor units is a more important factor for estimating the EOD than the capability of the spatial filter.

3.5. Which spatial filter configuration detects the MUAPs of two motor units with the greatest shape difference?

Table 3 presents the average and range of EOD values across all motor unit depths for different contact spacing values. The spatial filter configurations were ranked by their ability to maximize MUAP shape differences based on the overall average EOD value. The range of EOD values for each configuration reflects the values at the extreme depth differences. The two BiTDD configurations had the overall highest average EOD values (0.89), while the four LSD configurations had the lowest (0.75–0.78). These rankings do no change when configurations are ranked separately for each of the spacing values.

3.6. Which pair of array configurations detects the MUAP of a motor unit with the greatest difference in shape?

Making use of the symmetry of the simulation setup we calculated the EOD for 120 pair wise combinations of the 16 different spatial filter configurations that can be derived from the nine contact points. The combination of any LSD and any double differential configuration, of any TSD and any LSD, and of any TSD and any BiTDD configuration resulted in larger EOD values than all the other pairs. The EOD values from the pairs in which both array configurations were oriented in parallel were always smaller than those of pairs oriented perpendicularly.

A summary of the results of all pair wise combinations of spatial filter configurations is given in Table 4. Only the pairs with the 10 largest average EOD values are listed. The pair of 3TSD:2BiTDD always showed the greatest EOD values for all the depth differences investigated and its average EOD value was 39% higher than the second place, which was shared by two configuration pairs. Among the 10 pairs shown in Table 4, the pair of 3TSD:1BiTDD was least affected by motor unit depth differences (i.e., had the smallest EOD range) while the 4LSD:1TDD pair was the one most affected. In general, these results indicate that the EOD decreased with increasing motor unit depth. However, none of EOD values for any of the TSD:TDD pairs changed with varying motor unit depth and several pairs showed increas-

Table 3
Average and range of EOD values for all depth differences and electrode spacing values tested

Configuration	Average EOD	Range	Rank
1BiTDD	0.89	(0.32–1.00)	1
2BiTDD	0.89	(0.32–1.00)	1
5TSD	0.86	(0.25–1.00)	3
3TDD	0.86	(0.25–1.00)	3
1TSD	0.85	(0.24–1.00)	5
2TDD	0.85	(0.24–1.00)	5
3TSD	0.85	(0.23–1.00)	7
1TDD	0.85	(0.23–1.00)	7
NDD	0.85	(0.23–1.00)	7
2LDD	0.85	(0.22–1.00)	10
IB2	0.84	(0.22–1.00)	11
1LDD	0.83	(0.20–1.00)	12
1LSD	0.78	(0.16–0.99)	13
2LSD	0.78	(0.14–0.99)	14
3LSD	0.76	(0.13–0.99)	15
4LSD	0.75	(0.13–0.99)	16

Ranking is based on the ability to maximize EOD based on average of all the results. All EOD ranges were estimated by performing the calculation on two motor units whose depth difference ranged from $d = 1$ mm to $d = 10$ mm.

Table 4
The 10 configuration pairs with the greatest EOD values estimated from all configuration pairs of the nine-pin electrode array

Configuration pair	Average EOD (range)	Rank by EOD	Complexity (# electrodes)	Rank by complexity
3TSD:2BiTDD	1.64 (1.30–1.77)	1	8	10
3TSD:1BiTDD	1.33 (1.19–1.40)	2	6	6
4LSD:1TDD	1.33 (1.01–1.83)	2	5	3
2LSD:1TDD	1.32 (1.01–1.75)	4	5	3
1TSD:2BiTDD	1.30 (1.00–1.43)	5	6	6
1LDD:2BiTDD	1.24 (1.08–1.51)	6	7	9
2LSD:NDD	1.21 (0.91–1.43)	7	5	3
3TSD:4LSD	1.20 (1.01–1.59)	8	4	2
4LSD:NDD	1.19 (0.91–1.34)	9	6	6
2LSD:2LDD	1.18 (0.97–1.46)	10	3	1

The range of the EOD values is based on the simulation of 11 different motor unit depths (13–3 mm in 1 mm steps).

ing EOD with increasing depth (e.g. 1LSD:2TDD, 1LSD:2LDD, 1LSD:NDD, 1LSD:1BiTDD). Configuration pairs were also ranked by implementation complexity, which was measured in number of electrodes needed for signal detection. Note that four pairs involving a BiTDD configuration and requiring as little as six electrodes were among the top 10 EOD values. In contrast, the IB2 configuration, which requires all nine electrodes of the array, did not appear among the top 10 pairs (Table 4). Note that the simplest configuration pair among those with the top 10 largest EOD values, the 2LSD:2LDD combination, requires only the center row of three electrodes.

4. Discussion

Spatial filters can be described by various features such as gains, bandwidth, and signal to noise ratio, among others. We focused on the single parameter of the energy-of-difference (EOD) between the shapes of the motor unit action potential shapes because we were interested in identifying spatial filter configurations that would provide the most distinction amongst the detected action potentials. The algorithms that have proven to be successful for decomposing the superimposed sEMG signal rely heavily on the distinguishability of the shapes of the action potentials (De Luca et al., 2006). The greater the distinction amongst the action potential shapes, the greater the accuracy of the decomposition and the greater the number of motor unit action potential trains that can be identified in the superimposed EMG signal.

This study fixed the geometry of the volume conductor and the location of the electrode array on the surface of the skin to facilitate comparison of the performance of various spatial filters in distinguishing the action potentials of motor units located at different depth within the muscle. An extension of the results to different muscle geometries, tissue conductivities, or sensor locations needs to proceed with caution.

4.1. Maximum shape difference between two motor units

The results presented in Table 3 revealed that the BiTDD spatial filter provided the maximum energy difference (EOD) between the action potentials of two motor units located at different depths. This result is consistent with previous reports (Arabadzhier et al., 2003; Dimitrov et al., 2003) indicating high selectivity of the electrode array. Several studies (Dimitrov et al., 2003; Disselhorst-Klug et al., 1997; Farina and Cescon, 2001; Farina et al., 2002, 2003) assessed shape difference, or spatial filter selectivity, by measuring the MUAP amplitude and duration. While these parameters and the EOD show similar trends, there are several discrepancies. Several reports (Dimitrov et al., 2003; Disselhorst-Klug et al., 1997; Farina et al., 2003; Kostov et al., 1988) have indicated that the longitudinal selectivity of the detection system is reflected in the duration of the MUAP with shorter duration indicating higher selectivity. However, selectivity results were not consistent for a given set of spatial filter configurations (Dimitrov et al., 2003; Disselhorst-Klug et al., 1997), because the ability of the spatial filters to reduce the duration (or pick-up area) varied with the location of the motor unit below the skin (see also Table 2 of this study). A few studies assessed the transversal selectivity of the detection systems in terms of the amplitude attenuation (Dimitrov et al., 2003; Dimitrova et al., 1999; Farina et al., 2003; Helal and Bouissou, 1992). They concluded that the higher rate of amplitude attenuation indicated the higher selectivity of the detection system. For example, Dimitrov et al. (2003) indicated that LDD detection had always higher selectivity than TDD and NDD detection. However, this is not generally true. In the current study, the TDD and NDD configurations exhibited higher EOD values than the 1LDD (and 3LDD, due to symmetry), but lower than the 2LDD configuration (Fig. 4A).

Electrode spacing has also been investigated in the past. Some reports (Dimitrova et al., 1999; Farina et al., 2002; Fuglevand et al., 1992) indicated that larger spacing (wider pick-up area) contributes to lower selectivity. However, from a practical perspective, small spacing in a two-dimensional electrode array requires a small electrode/skin contact area (small pins) rendering the sensor sensitive to artifacts, thus limiting its usefulness. In line with previous results, Fig. 4A shows that decreasing the electrode spacing of array increased the EOD value and hence selectivity, but this effect was small. In comparison, the range of variation in the EOD value due to different motor unit depths (Fig. 4B) was much larger. Thus, for the given muscle architecture and the range of spacing values investigated in this study, electrode spacing was not a critical factor.

4.2. Maximum shape difference among pairs of array configurations

Pair wise combinations of spatial filter configurations were ranked by their ability to generate different MUAP shape representations for the same motor unit. We found the following dominant relationships:

(1) Out of the top 10 combinations ranked by EOD (see Table 4), four included BiTDD configurations, two of which ranked #1 and #2, while the remaining always included one LSD configuration.
(2) The EOD between any LSD and any TSD configuration was greater than that between all the other single differential filter pairs. This result indicates that difference in orientation of the spatial filters (i.e. longitudinal versus transversal) is an important factor that contributes to a high EOD value. The reason for this is that the MUAP shapes detected in each case are dramatically different. For example, the signal detected by a TSD spatial filter has a triphasic waveform and that detected by LSD has biphasic waveform (Fig. 3).
(3) The EOD of any SD:DD spatial filter pair (for example LSD:TDD) was always greater than that of any DD:DD pair because the double-differential configuration has a greater selectivity (Farina et al., 2003) (see Tables 2 and 3).

Thus, as for the results of the EOD values at different motor unit depths, the BiTDD spatial filter again stands out as the one that offers a highly distinguishable MUAP representation.

4.3. The proposed four-channel detection system for surface EMG decomposition

We identified design choices for the sensor based on the number of channels and the application in an EMG signal decomposition system. Given an electrode array of nine contact pins placed on a muscle in a fixed location, which spatial filter configuration should one choose to get the best one-channel sensor, i.e. the one that distinguishes between the action potentials of motor units located at different depths, and which additional spatial filter configurations (up to a total of four) should one chose to get the best multi-channel sensor, such that the representation of motor units in the channels is different.

For a one-channel detection system, where depth distinction matters primarily, either one of the two BiTDD configurations was always the best choice (Table 1). These configurations displayed the highest EOD values irrespective of motor unit depth and electrode spacing, within the limits of our simulation setup (Fig. 4).

When adding a second, third, and fourth channel, depth selectivity for each individual channel (i.e. the EOD values from Table 3) was weighed against inter-channel difference in MUAP shape representation (Table 4) in the following manner:

$$\text{Aggregate EOD} = (\text{Average EOD of configuration pairs}) + 1/2(\text{Average EOD of configurations})$$

Thus, the average inter-channel difference was weighted twice as high as the average depth selectivity. The resulting aggregate EOD values were ranked and the highest value chosen for our sensor design (Fig. 5). For a two-channel system, the combination 2BiTDD and 3TSD emerged as the preferred arrangement, which uses eight of the nine contact pins. For a three-channel system, the 1LSD configuration is added, again using eight out of nine electrodes. For a four-channel system, addition of the 1TDD configuration provides the highest aggregate EOD requiring all nine electrodes. It should be noted, that the second best two-channel arrangement was the combination 1BiTDD and 3TSD, which requires only six of the nine electrodes (Fig. 5, top right). The performance drop incurred by using only six pins to generate two EMG channels is 15% (1.768 versus 2.071 aggregate EOD). Fig. 5 indicates the four best configurations when one restricts the analysis to six electrodes, those of the 1BiTDD configuration, which makes for a sensor that occupies only half the contact area of the nine-electrode array (indicated by shaded circles in Fig. 5). Surprisingly, the same configurations for channels 2–4 are selected as in the case of a nine-electrode system. The difference in performance between the four-channel system that uses all nine electrodes and the one that uses only six is less than 5% (1.382 versus 1.319 aggregate EOD).

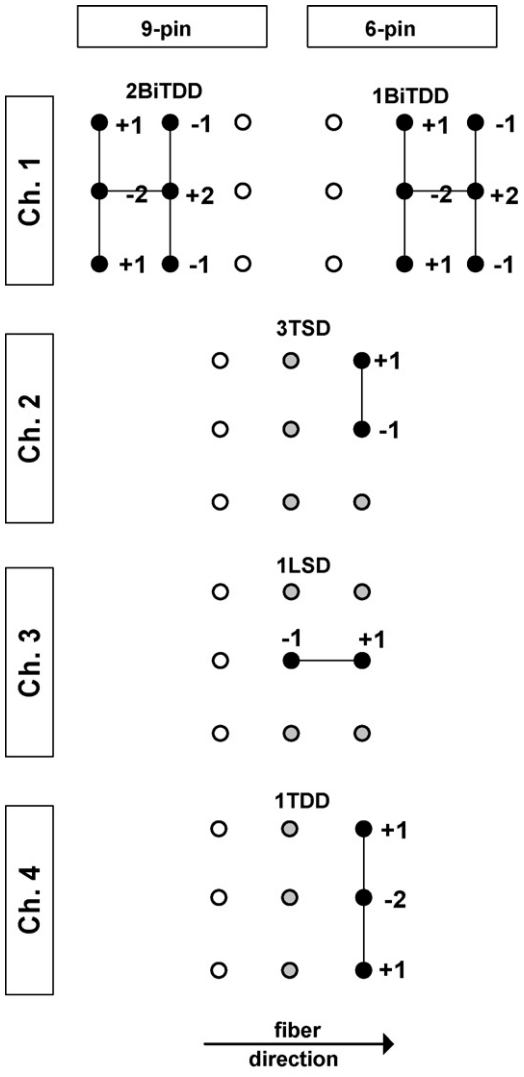

Fig. 5. Selection of spatial filter configurations for the proposed sensor system of up to four channels for application in SEMG decomposition. Shown are configurations based on a nine-pin (open circles) and six-pin (grey circles) electrode array for each of the four channels. Note that channels 2–4 are identical in both cases.

4.4. Concluding remarks

The issue of concern for this work was to identify spatial filter combinations that increased the distinction amongst detected action potentials. The decomposition algorithms which identify, track and assign the action potentials to a specific motor unit are not discussed in this document. Those algorithms have been described in numerous publications from our group during the past three decades. Recent references are: De Luca and Adam (1999), Nawab et al. (2004a,b), De Luca et al. (2006) and Sauvage et al. (2006). These algorithms are constructed from complex artificial intelligence constructs that involve a variety of signal analysis concepts. Among numerous other tasks, the algorithms track the changing shapes of the action potential that occur during a contraction as a consequence of the movement of the EMG sensor with respect to the location of the action potential source.

Acknowledgements

The authors graciously acknowledge the use of the ANVOLCON (Analytical Volume Conductor) Model developed by Joleen Blok and Dick Stegeman at the Department of Clin-

ical Neurophysiology, University Medical Center, Nijmegen, the Netherlands. This work was supported by the post-doctoral fellowship program of the Korean Science and Engineering Foundation (KOSEF), NICHD/NCMRR Bioengineering Research Partnership Grant HD38585, and NIH/NINDS grant NS058250 to Delsys Inc.

References

Adam A, De Luca CJ. Firing rates of motor units in human vastus lateralis muscle during fatiguing isometric contractions. J Appl Physiol 2005;99:268–80.

Andreassen S, Rosenfalck A. Recording from a single motor unit during strong effort. IEEE Trans Biomed Eng 1978;BME-25:501–8.

Arabadzhier TI, Dimitrov GV, Dimitrova NA. Simulation analysis of the ability to estimate motor unit propagation velocity non-invasively by different two-channel methods and types of multi-electrodes. J Electromyogr Kinesiol 2003;13:403–15.

Basmajian JV, De Luca CJ. Muscles alive; their functions revealed by electromyography. 5th ed. Baltimore, MD: William and Wilkins Co; 1985.

Blok JH, Stegeman DF, van Oosterom A. Three-layer volume conductor model and software package for applications in surface electromyography. Ann Biomed Eng 2002;30:313–26.

Broman H. Knowledge-based signal processing in the decomposition of myoelectric signals. IEEE Trans Eng Med Biol 1988;7:24–8.

De Luca CJ, Adam A.Windhorst U, Johansson H, editors. Decomposition and analysis of the intramuscular electromyographic signal. Modern techniques in neuroscience research. Heidelberg: Springer; 1999. p. 757–76.

De Luca CJ, Adam A, Wotiz R, Gilmore LD, Nawab SH. Decomposition of surface EMG signals. J Neurophysiol 2006;96:1646–57.

De Luca CJ, Forrest WJ. An electrode for recording single motor unit activity during strong muscle contractions. IEEE Trans Biomed Eng 1972;BME-19(5):367–72.

Dimitrov GV, Disselhorst-Klug C, Dimitrova NA, Schulte E, Rau G. Simulation analysis of the ability of different types of multielectrodes to increase selectivity of detection and to reduce cross-talk. J Electromyogr Kinesiol 2003;13:125–38.

Dimitrova NA, Dimitrov GV, Chihman VN. Effect of electrode dimensions on motor unit potentials. Med Eng Phys 1999;21:479–85.

Disselhorst-Klug C, Silny J, Rau G. Improvement of spatial resolution in surface EMG: a theoretical and experimental comparison of different spatial filters. IEEE Trans Biomed Eng 1997;BME-44:567–74.

Disselhorst-Klug C, Silny J, Rau G. Estimation of the relationship between noninvasively detected activity of single motor units and their characteristic pathological changes by modeling. J Electromyogr Kinesiol 1998;8: 323–35.

Erim Z, Beg MF, Burke D, De Luca CJ. Effects of aging on motor-unit control properties. J Neurophysiol 1999;82:2081–91.

Fang J, Agarwal GC, Shahani BT. Decomposition of multi-unit electromyographic signals. IEEE Trans Biomed Eng 1999;46:685–97.

Farina D, Arendt-Nielsen L, Merletti R, Indino B, Graven-Nielsen T. Selectivity of spatial filters for surface EMG detection from the tibialis anterior muscle. IEEE Trans Biomed Eng 2003;BME-50:354–64.

Farina D, Cescon C. Concentric ring electrode systems for noninvasive detection of single motor unit activity. IEEE Trans Biomed Eng 2001;BME-48:1326–34.

Farina D, Cescon C, Merletti R. Influence of anatomical and detection system parameters on surface EMG. Biol Cybern 2002;86:445–56.

Farina D, Mesin L, Martina S, Merletti R. Comparison of spatial filter selectivity in surface myoelectric signal detection: influence of the volume conductor model. Med Biol Eng Comput 2004;42:114–20.

Farina D, Merletti R. A novel approach for precise simulation of the EMG signal detected by surface electrodes. IEEE Trans Biomed Eng 2001;BME-46:637–46.

Farina D, Rainoldi A. Compensation of the effect of subcutaneous tissue layers on surface EMG: a simulation study. Med Eng Phys 1999;21:487–96.

Ferdjallah M, Wertsch JJ, Harris GG. Effect of surface electrode size on computer simulated surface motor unit potentials. Electromyogr Clin Neurophysiol 1999;39:259–65.

Fuglevand AJ, Winter DA, Patla AE, Stashuk D. Detection of motor unit action potentials with surface electrode: influence of electrode size and spacing. Biol Cybern 1992;67:143–53.

Griep P, Gielen F, Boon K, Hoogstraten L, Pool C, Wallinga de Jonge W. Calculation and registration of the same motor unit action potential. Electroencephalogr Clin Neurophysiol 1982;53:388–404.

Gydikov A, Gerilovsky L, Gatev P, Kostov K. Volume conduction of motor unit potentials from different human muscles to long distances. Electromyogr Clin Neurophysiol 1982;22:105–16.

Helal JN, Bouissou P. The spatial integration effect of surface electrode detecting myoelectric signal. IEEE Trans Biomed Eng 1992;BME-39:1161–7.

Hochstein L, Nawab SH, Wotiz R. An AI-based software architecture for a biomedical application. In: SCI-2002: proceedings of the 6th world multiconference on systemics, cybernetics and informatics, vol. XI; 2002. p. 60–4.

Kostov K, Gydikov A, Trayanova N, Kosarov D. Configuration and selectivity of the branched EMG electrodes. Electromyogr Clin Neurophysiol 1988;24:397–403.

LeFever RS, De Luca CJ. A procedure for decomposing the myoelectric signal into its constituent action potentials. Part I. Technique, theory and implementation. IEEE Trans Biomed Eng 1982;BME-29:149–57.

LeFever RS, Xenakis AP, De Luca CJ. A procedure for decomposing the myoelectric signal into its constituent action potentials. Part II. Execution and test for accuracy. IEEE Trans Biomed Eng 1982;BME-29:158–64.

Mambrito B, De Luca CJ. A technique for the detection, decomposition and analysis of the EMG signal. EEG Clin Neurophysiol 1984;58: 175–88.

Masuda T, Miyano H, Sadoyama T. The position of innervation zones in the biceps brachii investigated by surface electromyography. IEEE Trans Biomed Eng 1985;BME-32:36–42.

McGill KC, Cummins KL, Dorfman LJ. Automatic decomposition of the clinical electromyogram. IEEE Trans Biomed Eng 1985;32:470–7.

McGill KC, Lateva ZC, Xiao S. A model of the muscle action potential for describing the leading edge, terminal wave, and slow afterwave. IEEE Trans Biomed Eng 2001;BME-48:1357–65.

Merletti R, Lo Conte L, Avignone E, Guglielminotti P. Modeling of surface myoelectric signals. Part I. Model implementation. IEEE Trans Biomed Eng 1999a;BME-46:810–20.

Merletti R, Roy SH, Kupa E, Roatta S, Granata A. Modeling of surface myoelectric signals. Part II. Model based signal interpretation. IEEE Trans Biomed Eng 1999b;BME-46:821–9.

Nawab SH, Wotiz R, De Luca CJ. Resolving EMG pulse superpositions via utility maximization. In: Proceedings of the 8th world multiconference on systemics, cybernetics and informatics, vol. XII; 2004a. p. 233–6.

Nawab SH, Wotiz R, De Luca CJ. Improved resolution of pulse superpositions in a knowledge-based system for EMG decomposition. In: Proceedings of the 26th international conference of the IEEE engineering in medicine and biology society; 2004b. p. 69–71.

Oppenheim AV, Schafer RW. Digital signal processing. Englewood Cliffs, NJ: Prentice-Hall; 1975.

Östlund N, Yu J, Roeleveld K, Karlsson JS. Adaptive spatial filtering of multichannel surface electromyogram signals. Med Biol Eng Comput 2004;42:825–31.

Reucher H, Rau G, Silny J. Spatial filtering of noninvasive multielectrode EMG. Part I. Introduction to measuring technique and application. IEEE Trans Biomed Eng 1987a;BME-34:98–105.

Reucher H, Rau G, Silny J. Spatial filtering of noninvasive multielectrode EMG. Part II. Filter performance in theory and modeling. IEEE Trans Biomed Eng 1987b;BME-34:106–13.

Roeleveld K, Blok JH, Stegeman DF, van Oosterom A. Volume conduction model for surface EMG; confrontation with measurements. J Electromyogr Kinesiol 1997;7:221–32.

Sauvage C, Manto M, Adam A, Roark R, Jissendi P, De Luca CJ. Ordered motor unit firing behavior in acute cerebellar stroke. J Neurophysiol 2006;96:2769–74.

Schneider J, Silny J, Rau G. Influence of tissue inhomogeneities on non-invasive muscle fiber conduction velocity measurements investigated by physical and numerical modeling. IEEE Trans Biomed Eng 1991;BME-38: 851–60.

Stashuk D, de Bruin H. Automatic decomposition of selective needle-detected myoelectric signals. IEEE Trans Biomed Eng 1988;35:1–10.

Zennaro D, Wellig P, Moschytz GS, Läubli T, Krueger H. A decomposition software package for the decomposition of long-term multi-channel electromyographic signals. In: Proceedings of the 23rd annual international conference of the IEEE engineering in medicine and biology society; 2001. p. 1070–3.